

# LOCAL: A Graph-Based Active Learning Approach for Stability Analysis of DAC@NG Catalysts

Yue Yin <sup>†1</sup>, Jiangshan He<sup>†1</sup>, and Hai Xiao<sup>\*1</sup>

<sup>1</sup>Department of Chemistry, Tsinghua University, Beijing 100084, China

March 26, 2025

## Abstract

Dual atomic catalysts supported by nitrogen-doped graphene (DAC@NG) offer significant potential in catalytic applications by overcoming intrinsic limitations associated with single atomic catalysts. However, accurately determining their stability and atomic-scale configurations remains computationally challenging due to extensive structural variability. In this study, we present the LOCALization and Active Learning (LOCAL) framework, an innovative, scalable approach employing two graph convolutional network (GCN) models—POS2COHP and Graph2E—to predict stability energies directly from initial DAC@NG structures. Leveraging an extensive dataset of 611,648 DAC@NG structures, encompassing 38 metal elements, six distinct graphene quadra-vacancy patterns, and diverse carbon/nitrogen coordination environments, LOCAL achieved a remarkable validation mean absolute error of just 0.145 eV. Utilizing this framework, we systematically analyzed stability trends across various metal pairs, successfully generating phase diagrams for experimentally validated bimetallic systems (Co-Ni, Fe-Ni, Fe-Mn, and Ag-Ni). These results underscore LOCAL’s capability for rapidly evaluating structural stability, significantly accelerating the discovery and optimization of high-performance catalysts. The developed dataset and LOCAL framework are publicly available, offering a valuable resource for future catalyst design and broader exploration of catalytic materials.

## Introduction

The development of high-performance catalysts is essential for advancing sustainable chemical processes. Single atomic catalysts (SACs) have garnered significant interest due to their precise atomic structures and optimal atom utilization efficiency [1–12]. However, SACs exhibit intrinsic limitations, such as a

singular active site and restricted coordination environments, which constrain their catalytic versatility and performance [13–16].

Dual atomic catalysts (DACs), which pair two atomic active sites closely together, have emerged as a promising approach to overcoming these limitations [17–32]. By coupling two distinct metal atoms within defected nitrogen-doped graphene (NG), DACs significantly expand catalytic versatility through enhanced electronic interactions and richer coordination environments [33–45]. Despite their promising potential, accurately determining the stability and atomic-scale structure of DAC@NG systems remains a formidable challenge. Experimental methods such as extended X-ray absorption fine structure (EXAFS) and X-ray absorption near-edge structure (XANES) spectroscopy are valuable but often insufficiently precise for pinpointing exact atomic arrangements [46–48]. Conversely, conventional theoretical calculations, while precise, are computationally prohibitive for systematically evaluating the extensive combinatorial space of DAC structures [49].

To address these challenges, we present the LOCALization and Active Learning (LOCAL) framework, a scalable and efficient method capable of predicting stability energies directly from initial structures, thus bypassing expensive computations. We constructed a comprehensive dataset comprising 611,648 DAC@NG candidate structures, covering six distinct NG quadra-vacancy patterns and incorporating all combinations of 38 metal elements alongside varying carbon and nitrogen coordination arrangements. The LOCAL framework utilizes two graph convolutional network (GCN) models [50–63]: POS2COHP, which rapidly predicts integrated crystal orbital Hamilton population (ICOHP) values [64, 65] from initial structural inputs; and Graph2E, which integrates structural and ICOHP information to predict stability energies.

Trained on computationally derived stability energies, LOCAL achieved a validation mean absolute error of just 0.145 eV on a test set of more than 1,400 DAC@NG structures. Subsequently, LOCAL efficiently evaluated approximately 600,000 additional structures, enabling systematic exploration and identification of optimal DAC configurations. Leveraging these results, we successfully constructed phase diagrams for metal element pairs, exemplified by the Co-Ni, Fe-Ni, Fe-Mn, Ag-Ni pairs [66–69], which matched previously reported experimental data.

Our results demonstrate LOCAL’s efficacy as a powerful tool for predicting DAC@NG stability at scale, significantly accelerating the exploration and design of high-performance catalysts. To promote wider adoption and facilitate further catalyst development, we have made the dataset and LOCAL framework publicly available at [www.localenergy.science](http://www.localenergy.science).

Beyond DAC@NG structures, the LOCAL framework offers substantial potential for broader catalyst design challenges. Possible future expansions include the exploration of other graphene-based substrates doped with heteroatoms (e.g., O, S, P) and the integration of catalytic reaction intermediates and deeper electronic analyses, such as additional ICOHP values and Bader charges. Particularly effective in chemical spaces characterized by extensive local variability yet limited global structural diversity, LOCAL stands poised to significantly

impact the discovery and optimization of next-generation catalytic materials.

## Results and Discussion

### The DAC@NG Dataset

To ensure the LOCAL framework performs effectively, it is crucial to construct a carefully designed dataset with consistent structural distributions and a sufficient number of interconnected data points. Thus, we developed a comprehensive dataset systematically to represent dual atomic catalysts supported by nitrogen-doped graphene (DAC@NG).

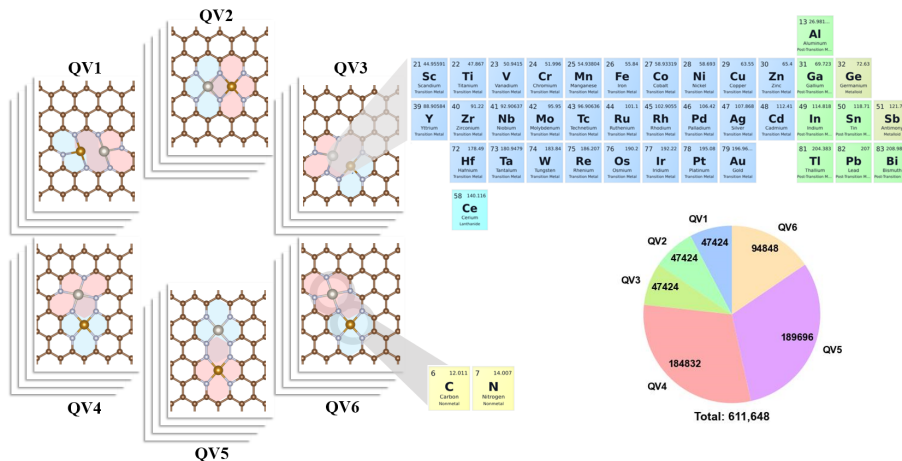


Figure 1: Construction of the DAC@NG Dataset.

We began by determining how to introduce four vacancies into the graphene structure. In typical single atomic catalyst (SAC@NG) systems, two adjacent carbon vacancies are introduced to anchor a single metal atom, creating a "normal hole" composed of four hexagons. To generate DAC@NG structures, we combined two SAC@NG units, ensuring their normal holes overlap by at least one shared hexagon. Following this criterion, we identified six distinct structural patterns, labeled QV1 through QV6, as illustrated in Fig. 1. Among these patterns, QV4 is uniquely asymmetric, requiring additional consideration for different permutations of the metal element pairs.

Next, we selected the metal elements to anchor into these vacancy structures. Considering that both transition and main group metals have demonstrated catalytic promise [70–77], our dataset included 38 metal elements. Specifically, we covered nearly all transition metals from the fourth, fifth, and sixth periods, excluding lanthanum (La) and mercury (Hg) but including cerium (Ce) as a representative lanthanide element. Main group metals were included up to bismuth (Bi), excluding alkali and alkaline earth metals. This extensive selection

ensures broad relevance and applicability for catalytic applications (see Fig. 1 for detailed elemental inclusion).

The dataset further accounted for variations in coordination environments at the edges of the vacancy holes, specifically focusing on carbon (C) and nitrogen (N) atoms. Nitrogen atoms generally exhibit stronger bonds (as reflected by higher ICOHP values) and often lead to higher metal oxidation states compared to carbon atoms. Since each QV pattern offers unique coordination possibilities, the dataset incorporated all possible permutations of C and N positions, resulting in a total of 611,648 unique candidate structures.

Due to practical limitations in calculating stability energies using conventional methods (as it is difficult to obtain precise reference energies for structures with four vacancies), we defined a modified stability energy that closely resembles formation energy. This energy was calculated as the difference between the total energy of the anchored DAC@NG structure and the summed chemical potentials of graphene, nitrogen, and the bulk metal atoms. To facilitate predicting stability directly from initial structures, we incorporated ICOHP values between the metal sites and their coordinating C/N atoms. ICOHP values quantify bond strengths, enabling the initial structures to effectively mimic the fully relaxed final structures without the need for computationally expensive density functional theory (DFT) calculations. QV2 and QV3 patterns required three ICOHP values per metal site, whereas QV1, QV4, QV5, and QV6 patterns required four due to their coordination numbers.

Finally, we initiated the LOCAL framework training through active learning. The initial training set (Loop 0) included carefully selected boundary-condition data points, specifically cases where the metal atoms are exclusively coordinated by either nitrogen or carbon atoms, providing a robust foundation. Additionally, random data points were chosen from various QV patterns and mixed C/N coordination scenarios to enhance generalization. Loop 0 contained 14,399 structures, followed by Loop 1 and loop 2 with additional 1,178 data points and 1,537 data points separately selected via active learning. This iterative refinement ensured continuous enhancement in model performance and generalizability. Detailed distributions of stability energies and ICOHP values for each loop are provided in the Supporting Information.

## The LOCAL Framework

To efficiently address the challenge of systematically determining stability energies for all DAC@NG structures in our extensive dataset, we developed an innovative computational framework termed LOCAL. This framework is specifically designed for datasets characterized by significant variability in local structural environments yet limited overall structural changes—a typical scenario exemplified by DAC@NG systems.

LOCAL introduces a hierarchical architecture named Chemistry-Informed Neural Networks (CINN), illustrated in Fig 2. CINN integrates two specialized Graph Convolutional Network (GCN) models: POS2COHP and Graph2E. By leveraging domain-specific chemical knowledge, CINN significantly enhances

predictive accuracy, especially in systems with intricate local chemical environments.

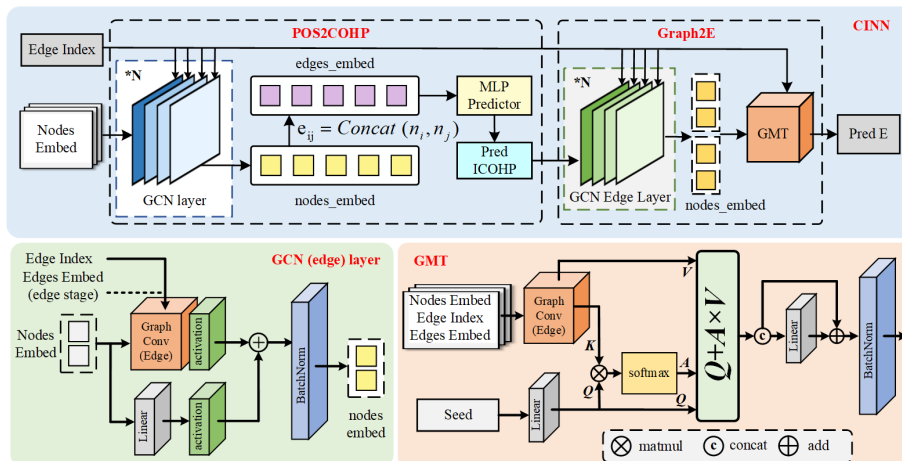


Figure 2: The CINN architecture.

The POS2COHP model predicts integrated crystal orbital Hamilton population (ICOHP) values, quantifying bond strengths based on initial structural representations. These initial structures derive from six fundamental quadravacancy (QV) patterns of graphene, where nitrogen doping occurs at the edges and two metal atoms occupy designated vacancy sites. Coordination environments around these metal sites can vary between carbon (C) and nitrogen (N) atoms. To ensure structural consistency, each C/N atom bonds with three neighbors, whereas metal atoms bond with three or four C/N atoms, depending on the QV pattern. Atomic positions remain constant within each QV pattern, varying only in the elemental identity of coordinating atoms and metal sites, changing the node representations in the graph inputs. Node embeddings utilize one-hot encoding, with no explicit edge attributes. Multiple GCN layers process these embeddings, concatenating metal and coordinating atom embeddings to form bond representations, which are subsequently processed by a multi-layer perceptron (MLP) to predict ICOHP values.

These predicted ICOHP values, combined with the original graph representations, serve as inputs for the Graph2E model. Graph2E incorporates ICOHP predictions as edge attributes, effectively mimicking graphs derived from fully relaxed final structures. Utilizing GCN layers that integrate edge attributes, Graph2E facilitates comprehensive message-passing between nodes. To capture complex global interactions within each structure, a transformer-based pooling layer is employed, generating a 256-dimensional embedding vector that encapsulates global structural features. This embedding vector, further processed through an MLP, predicts the structure’s stability energy. Due to the active learning integration, the transformer pooling layer also acts as a decoder, pro-

viding embeddings crucial for subsequent active learning cycles.

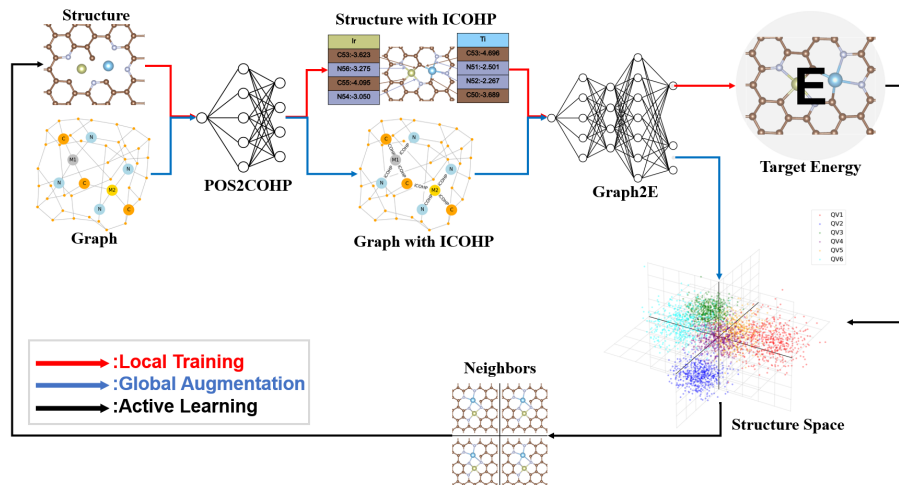


Figure 3: The overall workflow of LOCAL.

As depicted in Fig 3, the overall workflow of LOCAL comprises three main stages: Local Training, Global Augmentation, and Active Learning. Each stage is meticulously designed to ensure efficient and accurate prediction of stability energies for DAC@NG structures.

In the Local Training stage, the two models POS2COHP and Graph2E within the CINN are sequentially trained using the initial training set. This subset contains DFT-calculated ICOHP values and corresponding stability energies. Initially, the POS2COHP model learns to predict ICOHP values from the graph representation of the initial DAC@NG structures. These predictions, alongside the initial structure graphs, form the input for the Graph2E model. Graph2E, trained subsequently, predicts the stability energies of these structures. Throughout this training stage, the performance of both models is assessed to identify data points exhibiting high prediction errors, which are subsequently targeted for improvement.

In the Global Augmentation stage, the trained models are applied to the entire dataset to perform systematic predictions. Specifically, the Graph2E model processes the graph representations to extract high-dimensional embeddings from its penultimate layer. These embeddings, each a 256-dimensional vector, collectively populate a high-dimensional embedding space. This embedding space is structured using KDTree algorithms, enabling efficient and precise identification of structurally similar data points and facilitating comprehensive similarity analyses across the entire dataset.

The Active Learning stage is crucial for enhancing model accuracy, especially for data points initially challenging to predict accurately. Here, data points with the highest prediction errors (top 10%) identified in the Local Training stage are

selected. Their corresponding high-dimensional embeddings serve as reference points to find structurally analogous neighbors within the embedding space. The similarity between structures is quantified using the Euclidean distance:

$$d_{x,y} = \sqrt{\sum_{i=1}^D (x_i - y_i)^2} \quad (1)$$

where  $x$  and  $y$  represent high-dimensional embedding vectors, and  $D$  is the embedding dimension. Neighbor selection follows error-based criteria: three neighbors for errors  $\leq 1.5$  eV, two neighbors for errors between 1.0–1.5 eV, and one neighbor for errors between 0.2–1.0 eV. Structures below a 0.2 eV error do not yield neighbors. Selected structures undergo additional DFT calculations to refine the model iteratively, continuing until the mean absolute error (MAE) of the worst-performing 10% of data points falls below 0.2 eV [78, 79].

In summary, the LOCAL framework effectively integrates localized chemical knowledge extraction, global structural feature representation, and active learning strategies. Its modular design facilitates straightforward adaptation to evolving computational methodologies, making it broadly applicable to catalyst discovery and database enhancement tasks.

## Resulting Stability Energy Predictions

In this section, we analyze the predicted stability energies of DAC@NG structures, providing insights into the overall distribution patterns, dependencies on metal pair selection, and the influence of different QV patterns. Through integrated analysis using the stability energy histogram and heatmap Fig.4, we elucidate key factors affecting catalyst stability, thereby guiding future catalyst design and optimization.

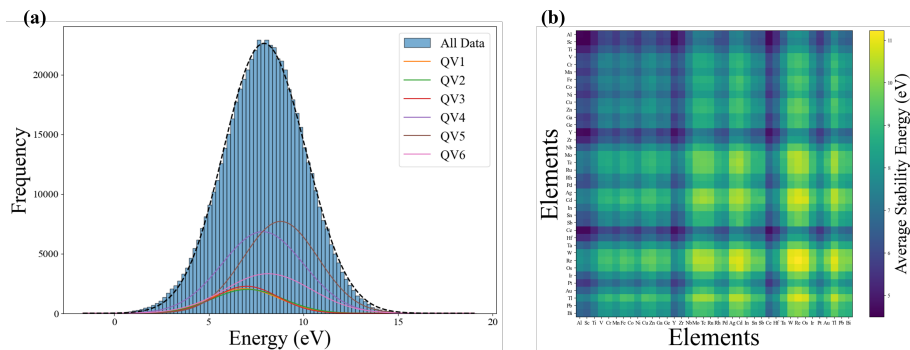


Figure 4: (a) Distribution of predicted stability energy for the DAC@NG dataset; (b) Heatmap of predicted stability energies for element pairs.

Fig.4(a) presents the stability energy histogram of the complete dataset, revealing a single-peaked distribution with energies spanning from -1.65 eV to

19.03 eV. The majority of structures cluster within intermediate energy ranges, indicating that extreme values (either significantly low or high energies) are relatively rare. This distribution suggests most DAC configurations possess moderate stability, with only a small subset exhibiting highly favorable stability (low energies). For deeper insights, the dataset is further subdivided according to the six distinct QV patterns (QV1 to QV6), allowing comparative analysis of their respective impacts on stability.

The detailed analysis by QV pattern highlights notable differences:

QV1 structures exhibit stability energies ranging from 0.25 eV to 13.06 eV, with a median of 6.87 eV. The distribution indicates relatively favorable stability across various metal pair combinations. QV2 and QV3 display similar energy ranges to QV1. However, QV2 notably contains the structure with the lowest observed energy (QV2\_Sc\_Sc), whereas QV3 features a narrower distribution (lower variance), suggesting stronger metal-metal interactions due to closer proximity between metal sites. QV4, QV5, and QV6 exhibit broader energy distributions. Specifically, QV4 ranges from -0.93 eV to 18.34 eV, QV5 from 1.23 eV to 19.03 eV, and QV6 from -1.56 eV to 18.22 eV. The highest energy observed is within QV5 (e.g., QV5\_01234567\_Re\_Pb), attributed to increased structural variability and complexity arising from greater coordination possibilities.

To further elucidate the stability trends among metal pairs, Fig.4(b) shows a heatmap of average stability energies for each element combination. Most metal pairs demonstrate average energies between approximately 4.6 eV and 10 eV. Lower energies typically correlate with lighter metals (e.g., Al, Sc), while heavier metals (e.g., Au, Pb, Bi) generally yield higher energies, likely due to steric interactions and atomic size differences. Notably, specific metal combinations involving elements like Y, Ce, and Pt exhibit unexpectedly lower average energies compared to neighboring elements, suggesting distinct coordination or interaction mechanisms enhancing local stability.

Figure 5 presents the phase evolution behavior of four representative bimetallic catalytic systems—(a) Co-Ni, (b) Fe-Ni, (c) Fe-Mn, and (d) Ag-Ni—under conditions of fixed carbon chemical potential (corresponding to the central values on the x-axis) and varying nitrogen chemical potential. Systematic investigations demonstrate that the central phases appearing in these diagrams (QV6\_Co\_Ni, QV2\_Fe\_Ni, QV2\_Fe\_Mn, and QV2\_Ag\_Ni) have all been successfully synthesized and experimentally confirmed [34, 66, 68, 69]. These experimental results exhibit excellent agreement with predictions from the LOCAL framework, strongly validating the accuracy and reliability of the constructed phase diagrams.

Detailed analysis reveals that as the nitrogen chemical potential decreases, a clear trend emerges wherein the nitrogen content within each system progressively diminishes, transitioning systematically from high-nitrogen structures to nitrogen-poor configurations. Although numerous theoretically feasible phases exist, only a select few are thermodynamically favorable and thus potentially synthesizable. However, practical synthesis additionally depends on kinetic factors, which are not considered in this analysis. Certain predicted structures,



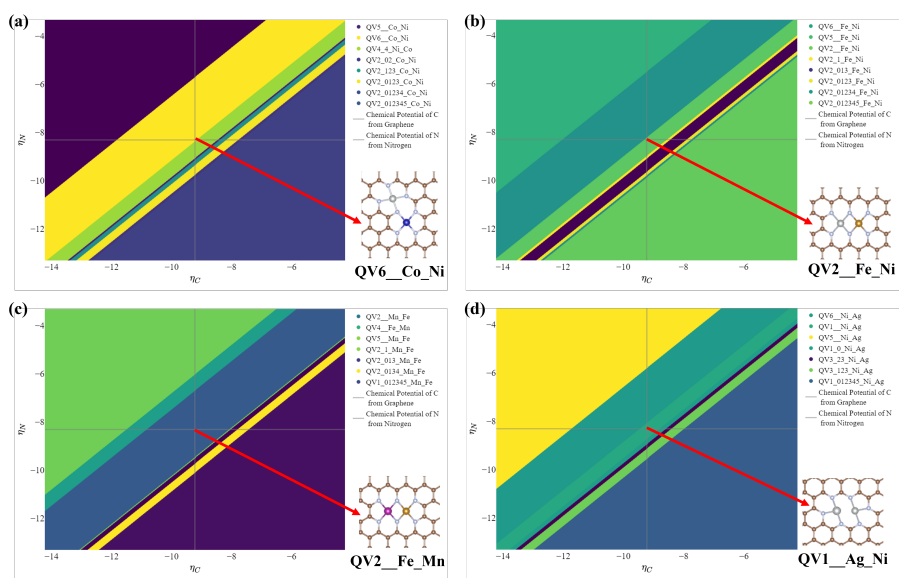


Figure 5: Examples of phase diagrams for bimetallic catalysts. (a) Phase diagram of the Co-Ni bimetallic catalyst with QV6\_Co\_Ni as the dominant phase; (b) Phase diagram of the Fe-Ni bimetallic catalyst with QV2\_Fe\_Ni as the dominant phase; (c) Phase diagram of the Fe-Mn bimetallic catalyst with QV2\_Fe\_Mn as the dominant phase; (d) Phase diagram of the Ag-Ni bimetallic catalyst with QV1\_Ag\_Ni as the dominant phase.

despite being thermodynamically plausible, might not form experimentally due to kinetic constraints. This phenomenon highlights the critical role of thermodynamics in determining structural stability, while also underscoring the necessity of incorporating kinetic considerations in practical experimental studies.

Furthermore, this synergistic approach between theory and experiment significantly deepens the understanding of phase evolution mechanisms in catalytic systems, providing precise guidance and reliable references for future catalyst design and optimization. While existing studies on dual-atom catalysts (DAC) have primarily focused on systems containing Fe, Co, and Ni, there remains considerable potential to explore a broader chemical space. Expanding investigations into additional transition metals and metal combinations could further enrich the design principles derived from phase diagram analysis, making it an even more powerful tool for guiding experimental efforts and optimizing catalytic material performance.

This study has established a comprehensive database of bimetallic phase diagrams covering all 38 transition metals, encompassing a total of  $C(38,2) = 741$  unique phase diagrams. The database offers interactive visualization capabilities, enabling users to dynamically select pairs of metals to generate corresponding phase diagrams, adjust chemical potential ranges to explore specific phases, and access detailed structural representations of key phases. The database is accessible at [www.localenergy.science/phasediagrams.html](http://www.localenergy.science/phasediagrams.html).

## Conclusion

In conclusion, the LOCAL framework introduced in this study represents a powerful and scalable computational tool for systematically predicting stability energies of dual atomic catalysts supported by nitrogen-doped graphene (DAC@NG). By leveraging two specialized graph convolutional network models—POS2COHP for predicting bond strengths (ICOHP values) and Graph2E for stability energy estimation—LOCAL successfully addressed the computational challenges posed by an extensive dataset comprising 611,648 DAC@NG candidate structures. The comprehensive dataset encompassed diverse coordination environments, 38 metal elements, and six distinct graphene vacancy patterns, ensuring broad applicability across catalytic systems.

The framework achieved remarkable predictive accuracy, validated by a mean absolute error of only 0.145 eV on an extensive test set. Furthermore, phase diagrams generated by LOCAL for selected metal pairs, such as Co-Ni, Fe-Ni, Fe-Mn, and Ag-Ni, exhibited excellent agreement with experimental observations, confirming its effectiveness and reliability.

The study underscores the importance of integrating theoretical calculations with experimental validation to deepen our understanding of catalytic phase evolution. While existing research has primarily concentrated on DACs involving Fe, Co, and Ni, significant opportunities remain for exploring broader chemical spaces. The publicly accessible DAC@NG database established herein facilitates further exploration and design optimization, serving as a valuable resource for

the catalysis research community.

Ultimately, LOCAL demonstrates substantial potential for wider applications, extending beyond DAC@NG systems to other catalytic materials. Future directions may include exploring alternative substrates and incorporating more comprehensive electronic analyses. Through such expansions, LOCAL will continue to significantly advance the design and discovery of next-generation high-performance catalytic materials.

## Data Availability

The whole dataset in this work is available on <https://www.localenergy.science>.  
The TOSS code and ML models are available on <https://github.com/yueyin19960520/LOCAL>.

## Corresponding Author

\*Corresponding author. E-mail: haixiao@tsinghua.edu.cn

## Acknowledgements

This work was supported by National Natural Science Foundation of China (Nos. 22122304 and 92261111), the NSFC Center for Single-Atom Catalysis (22388102), and National Key Research and Development Project (2022YFA1503000). We are also grateful to the Center of High-Performance Computing at Tsinghua University for providing computational resources.

## References

- [1] S. K. Kaiser, Z. Chen, D. Faust Akl, et al. Single-atom catalysts across the periodic table. *Chem. Rev.*, 120(21):11703–11809, 2020.
- [2] X. F. Yang, A. Wang, B. Qiao, et al. Single-atom catalysts: a new frontier in heterogeneous catalysis. *Acc. Chem. Res.*, 46(8):1740–1748, 2013.
- [3] L. Li, X. Chang, X. Lin, et al. Theoretical insights into single-atom catalysts. *Chem. Soc. Rev.*, 49(22):8156–8178, 2020.
- [4] A. Wang, J. Li, and T. Zhang. Heterogeneous single-atom catalysis. *Nat. Rev. Chem.*, 2(6):65–81, 2018.
- [5] L. Li, K. Yuan, and Y. Chen. Breaking the scaling relationship limit: from single-atom to dual-atom catalysts. *Acc. Mater. Res.*, 3(6):584–596, 2022.
- [6] B. Qiao, A. Wang, X. Yang, et al. Single-atom catalysis of co oxidation using  $\text{pt}_1/\text{feo}_x$ . *Nat. Chem.*, 3(8):634–641, 2011.

- [7] J. Li, Y. Li, and T. Zhang. *Recent progresses in the research of single-atom catalysts*. Springer, 2020.
- [8] H. Xiao, III Goddard, W. A., T. Cheng, et al. Cu metal embedded in oxidized matrix catalyst to promote  $\text{CO}_2$  activation and CO dimerization for electrochemical reduction of  $\text{CO}_2$ . *Proc. Natl. Acad. Sci. U.S.A.*, 114(26):6685–6688, 2017.
- [9] Z. Miao, S. Li, C. Priest, et al. Effective approaches for designing stable m–nx/c oxygen-reduction catalysts for proton-exchange-membrane fuel cells. *Adv. Mater.*, 34(52):2200595, 2022.
- [10] Y. Li, H. Wang, C. Priest, et al. Advanced electrocatalysis for energy and environmental sustainability via water and nitrogen reactions. *Adv. Mater.*, 33(6):e2000381, 2021.
- [11] Q. Li, W. Chen, H. Xiao, et al. Fe isolated single atoms on s, n codoped carbon by copolymer pyrolysis strategy for highly efficient oxygen reduction reaction. *Adv. Mater.*, 30(25):e1800588, 2018.
- [12] Y. Wang, X. Zheng, and D. Wang. Design concept for electrocatalysts. *Nano Res.*, pages 1–23, 2022.
- [13] J. Jiao, R. Lin, S. Liu, et al. Copper atom-pair catalyst anchored on alloy nanowires for selective and efficient electrochemical reduction of  $\text{CO}_2$ . *Nat. Chem.*, 11(3):222–228, 2019.
- [14] Y. Pan, C. Zhang, Z. Liu, et al. Structural regulation with atomic-level precision: From single-atomic site to diatomic and atomic interface catalysis. *Matter*, 2(1):78–110, 2020.
- [15] Y. Ying, X. Luo, J. Qiao, et al. “more is different:” synergistic effect and structural engineering in double-atom catalysts. *Adv. Funct. Mater.*, 31(3):2007423, 2021.
- [16] Z. Chen, L. Chen, C. Yang, et al. Atomic (single, double, and triple atoms) catalysis: frontiers, opportunities, and challenges. *J. Mater. Chem. A*, 7(8):3492–3515, 2019.
- [17] T. He, A. R. P. Santiago, Y. Kong, et al. Atomically dispersed heteronuclear dual-atom catalysts: A new rising star in atomic catalysis. *Small*, 18(12):e2106091, 2022.
- [18] X. Lv, W. Wei, B. Huang, et al. High-throughput screening of synergistic transition metal dual-atom catalysts for efficient nitrogen fixation. *Nano Lett.*, 21(4):1871–1878, 2021.
- [19] T. Pu, J. Ding, F. Zhang, et al. Dual atom catalysts for energy and environmental applications. *Angew. Chem. Int. Ed. Engl.*, 62(40):e202305964, 2023.

- [20] M. K. Wong, J. J. Foo, J. Y. Loh, et al. Leveraging dual-atom catalysts for electrocatalysis revitalization: exploring the structure-performance correlation. *Adv. Energy Mater.*, 14(18):2303281, 2024.
- [21] Y. Cheng, C. Shao, and W. Wang. Rational modulate the coordination environment of femonx-g electrocatalysts to boost nitrogen reduction reaction activity. *Molecular Catalysis*, 572:114757, 2025.
- [22] M. A. Akhound, M. Soleimani, and M. Pourfath. Tunable  $n_2$  fixation enabled by ferroelectric switching in doped graphene/ $in_2se_3$  dual-atom catalysts. *ACS Appl. Mater. Interfaces*, 2025.
- [23] C. Zhang, S. Qin, B. Li, et al. Dual-metal atom incorporated n-doped graphenes as oxygen evolution reaction electrocatalysts: high activities achieved by site synergies. *J. Mater. Chem. A*, 10(15):8309–8323, 2022.
- [24] Q. An, J. Jiang, W. Cheng, et al. Recent advances in dual-atom site catalysts for efficient oxygen and carbon dioxide electrocatalysis. *Small Methods*, 6(7):e2200408, 2022.
- [25] R. Li, Z. Zhang, X. Liang, et al. Polystyrene waste thermochemical hydrogenation to ethylbenzene by a n-bridged co, ni dual-atom catalyst. *J. Am. Chem. Soc.*, 145(29):16218–16227, 2023.
- [26] Y. Gao, B. Liu, and D. Wang. Microenvironment engineering of single/dual-atom catalysts for electrocatalytic application. *Adv. Mater.*, 35(31):e2209654, 2023.
- [27] J. Yang, Q. Liu, S. Chen, et al. Single-atom and dual-atom electrocatalysts: Synthesis and applications. *ChemPlusChem*, 88(10):e202300407, 2023.
- [28] Y. Zhang, T. Liu, X. Wang, et al. Dual-atom metal and nonmetal site catalyst on a single nickel atom supported on a hybridized bcn nanosheet for electrochemical  $co_2$  reduction to methane: Combining high activity and selectivity. *ACS Appl. Mater. Interfaces*, 14(7):9073–9083, 2022.
- [29] H. Zhu, Z. Guo, D. Lan, et al. Accelerating the design of catalysts for  $co_2$  electroreduction to hcooh: A data-driven dft-ml screening of dual atom catalysts. *J. Energy Chem.*, 99:627–635, 2024.
- [30] H. Zhang, Q. Wei, S. Wei, et al. Machine learning assisted screening of nitrogen-doped graphene-based dual-atom hydrogen evolution electrocatalysts. *Molecular Catalysis*, 570:114649, 2025.
- [31] B. Wang, C. Cheng, M. Jin, et al. A site distance effect induced by reactant molecule matchup in single-atom catalysts for fenton-like reactions. *Angew. Chem. Int. Ed. Engl.*, 61(33):e202207268, 2022.
- [32] Y. Li, B. Wei, M. Zhu, et al. Synergistic effect of atomically dispersed ni-zn pair sites for enhanced  $co_2$  electroreduction. *Adv. Mater.*, 33(41):e2102212, 2021.

- [33] W. Ye, S. Chen, Y. Lin, et al. Precisely tuning the number of fe atoms in clusters on n-doped carbon toward acidic oxygen reduction reaction. *Chem*, 5(11):2865–2878, 2019.
- [34] G. Yang, J. Zhu, P. Yuan, et al. Regulating fe-spin state by atomically dispersed mn-n in fe-nc catalysts with high oxygen reduction activity. *Nat. Commun.*, 12(1):1734, 2021.
- [35] C. H. Chen, D. Wu, Z. Li, et al. Ruthenium-based single-atom alloy with high electrocatalytic activity for hydrogen evolution. *Adv. Energy Mater.*, 9(20):1803913, 2019.
- [36] Y. S. Wei, L. Sun, M. Wang, et al. Fabricating dual-atom iron catalysts for efficient oxygen evolution reaction: A heteroatom modulator approach. *Angew. Chem. Int. Ed. Engl.*, 59(37):16013–16022, 2020.
- [37] L. Zhang, J. Fischer, Y. Jia, et al. Coordination of atomic co-pt coupling species at carbon defects as active sites for oxygen reduction reaction. *J. Am. Chem. Soc.*, 140(34):10757–10763, 2018.
- [38] X. Guo, J. Gu, S. Lin, et al. Tackling the activity and selectivity challenges of electrocatalysts toward the nitrogen reduction reaction via atomically dispersed biatom catalysts. *J. Am. Chem. Soc.*, 142(12):5709–5721, 2020.
- [39] Z. Zeng, L. Y. Gan, H. Bin Yang, et al. Orbital coupling of hetero-diatom nickel-iron site for bifunctional electrocatalysis of co(2) reduction and oxygen evolution. *Nat. Commun.*, 12(1):4088, 2021.
- [40] Y. Sun, J. Wang, Q. Liu, et al. Itinerant ferromagnetic half metallic cobalt–iron couples: promising bifunctional electrocatalysts for orr and oer. *J. Mater. Chem. A*, 7(47):27175–27185, 2019.
- [41] M. Xiao, Y. Chen, J. Zhu, et al. Climbing the apex of the orr volcano plot via binuclear site construction: Electronic and geometric engineering. *J. Am. Chem. Soc.*, 141(44):17763–17770, 2019.
- [42] Z. Lu, B. Wang, Y. Hu, et al. An isolated zinc-cobalt atomic pair for highly active and durable oxygen reduction. *Angew. Chem. Int. Ed. Engl.*, 58(9):2622–2626, 2019.
- [43] F. Li and Z. Chen. Cu dimer anchored on c(2)n monolayer: low-cost and efficient bi-atom catalyst for co oxidation. *Nanoscale*, 10(33):15696–15705, 2018.
- [44] Y. Li, H. Su, S. H. Chan, et al. Co<sub>2</sub> electroreduction performance of transition metal dimers supported on graphene: a theoretical study. *ACS Catal.*, 5(11):6658–6664, 2015.
- [45] H. Yan, Y. Lin, H. Wu, et al. Bottom-up precise synthesis of stable platinum dimers on graphene. *Nat. Commun.*, 8(1):1070, 2017.

- [46] J. E. Penner-Hahn. X-ray absorption spectroscopy in coordination chemistry. *Coord. Chem. Rev.*, 190:1101–1123, 1999.
- [47] J. Yano and V. K. Yachandra. X-ray absorption spectroscopy. *Photosynth. Res.*, 102(2-3):241–254, 2009.
- [48] J. Rehr and A. Ankudinov. Progress in the theory and interpretation of xanes. *Coord. Chem. Rev.*, 249(1-2):131–140, 2005.
- [49] J. Xu, X. M. Cao, and P. Hu. Perspective on computational reaction prediction using machine learning methods in heterogeneous catalysis. *Phys. Chem. Chem. Phys.*, 23(19):11155–11179, 2021.
- [50] L. Breiman. Random forests. *Machine Learning*, 45:5–32, 2001.
- [51] T. N. Kipf and M. Welling. Semi-supervised classification with graph convolutional networks. *arXiv:1609.02907*, 2016.
- [52] F. Scarselli, M. Gori, A. C. Tsoi, et al. The graph neural network model. *IEEE Transactions on Neural Networks*, 20(1):61–80, 2009.
- [53] K. Schütt, P.-J. Kindermans, F. H. E. Sauceda, et al. SchNet: A continuous-filter convolutional neural network for modeling quantum interactions. In *Advances in Neural Information Processing Systems*, volume 30, 2017.
- [54] S. Zhang, H. Tong, J. Xu, et al. Graph convolutional networks: a comprehensive review. *Computational Social Networks*, 6(1):11, 2019.
- [55] X. Glorot, A. Bordes, and Y. Bengio. Deep sparse rectifier neural networks. In *Proceedings of the Fourteenth International Conference on Artificial Intelligence and Statistics*, pages 315–323, 2011.
- [56] D. P. Kingma and J. Ba. Adam: A method for stochastic optimization. *arXiv:1412.6980*, 2014.
- [57] T. N. Kipf and M. Welling. Variational graph auto-encoders. *arXiv:1611.07308*, 2016.
- [58] W. Hamilton, Z. Ying, and J. Leskovec. Inductive representation learning on large graphs. In *Advances in Neural Information Processing Systems*, volume 30, 2017.
- [59] P. Veličković, G. Cucurull, A. Casanova, et al. Graph attention networks. *arXiv:1710.10903*, 2017.
- [60] A. Vaswani, N. Shazeer, N. Parmar, et al. Attention is all you need. In *Advances in Neural Information Processing Systems*, volume 30, 2017.
- [61] K. Han, A. Xiao, E. Wu, et al. Transformer in transformer. In *Advances in Neural Information Processing Systems*, volume 34, pages 15908–15919, 2021.

- [62] L. Rampásek, M. Galkin, V. P. Dwivedi, et al. Recipe for a general, powerful, scalable graph transformer. In *Advances in Neural Information Processing Systems*, volume 35, pages 14501–14515, 2022.
- [63] S. Yun, M. Jeong, R. Kim, et al. Graph transformer networks. In *Advances in Neural Information Processing Systems*, volume 32, 2019.
- [64] R. Nelson, C. Ertural, J. George, et al. Lobster: Local orbital projections, atomic charges, and chemical-bonding analysis from projector-augmented-wave-based density-functional theory. *Journal of Computational Chemistry*, 41(21):1931–1940, 2020.
- [65] S. Maintz, V. L. Deringer, A. L. Tchougréeff, et al. Lobster: A tool to extract chemical bonding from plane-wave based dft. Wiley Online Library, 2016.
- [66] R. Li, Z. Zhang, X. Liang, et al. Polystyrene waste thermochemical hydrogenation to ethylbenzene by a n-bridged co, ni dual-atom catalyst. *Journal of the American Chemical Society*, 145(29):16218–16227, 2023.
- [67] G. Yang, J. Zhu, P. Yuan, et al. Regulating fe-spin state by atomically dispersed mn-n in fe-nc catalysts with high oxygen reduction activity. *Nature Communications*, 12(1):1734, 2021.
- [68] Z. Zeng, L. Y. Gan, H. Bin Yang, et al. Orbital coupling of hetero-diatomic nickel-iron site for bifunctional electrocatalysis of co2 reduction and oxygen evolution. *Nature Communications*, 12(1):4088, 2021.
- [69] Z. Guo, H. Zhu, G. Yang, et al. Synergistic engineering of heteronuclear ni-ag dual-atom catalysts for high-efficiency co2 electroreduction with nearly 100% co selectivity. *Chemical Engineering Journal*, 476:146556, 2023.
- [70] H. Hu, J. Wang, B. Cui, and et al. Atomically dispersed selenium sites on nitrogen-doped carbon for efficient electrocatalytic oxygen reduction. *Angewandte Chemie International Edition*, 61(3):e202114441, 2022.
- [71] T. Wang, Q. Wang, Y. Wang, and et al. Atomically dispersed semimetallic selenium on porous carbon membrane as an electrode for hydrazine fuel cells. *Angewandte Chemie International Edition*, 58(38):13466–13471, 2019.
- [72] S. Liu, Z. Li, C. Wang, and et al. Turning main-group element magnesium into a highly active electrocatalyst for oxygen reduction reaction. *Nature Communications*, 11(1):938, 2020.
- [73] M. Sun, H. H. Wong, T. Wu, and et al. Stepping out of transition metals: activating the dual atomic catalyst through main group elements. *Advanced Energy Materials*, 11(30):2101404, 2021.



- [74] C. Wang, Y. Han, M. Tian, and et al. Main-group catalysts with atomically dispersed in sites for highly efficient oxidative dehydrogenation. *Journal of the American Chemical Society*, 144(37):16855–16865, 2022.
- [75] T. Wang, Y. Sun, G. Fu, and et al. Progress of main-group metal-based single-atom catalysts. *Electrochemical Energy Reviews*, 7(1):29, 2024.
- [76] F. Luo, A. Roy, L. Silvioli, and et al. P-block single-metal-site tin/nitrogen-doped carbon fuel cell cathode catalyst for oxygen reduction reaction. *Nature Materials*, 19(11):1215–1223, 2020.
- [77] T. Wang, X. Cao, H. Qin, and et al. P-block atomically dispersed antimony catalyst for highly efficient oxygen reduction reaction. *Angewandte Chemie International Edition*, 60(39):21237–21241, 2021.
- [78] Axel D. Becke. Density-functional thermochemistry. III. the role of exact exchange. *The Journal of Chemical Physics*, 98(7):5648–5652, 1993.
- [79] J. Heyd, G. E. Scuseria, and M. Ernzerhof. Hybrid functionals based on a screened coulomb potential. *The Journal of Chemical Physics*, 118(18):8207–8215, 2003.